Hindawi
Geofluids
Volume 2023, Article ID 3195453, 15 pages
https://doi.org/10.1155/2023/3195453

Research Article

Analysis of Shear Stagger Deformation of Existing Shield Tunnel below Induced by Quasirectangular Shield Tunneling

Kun Zhang, Xi Chen, Wei Yin, Kun Hu, and ShengXue Zhu

Huaiyin Institute of Technology, Huaian, Jiangsu 223003, China

Correspondence should be addressed to Xi Chen; zhaoyb@csu.edu.cn

Received 9 October 2022; Revised 25 October 2022; Accepted 24 November 2022; Published 25 January 2023

Academic Editor: Dongjiang Pan

To use urban underground space more efficiently is a research hotspot of urban underground development. Compared with conventional circular tunnels, quasirectangular tunnels have the characteristics of larger space utilization and higher economic benefits, gradually used in urban rail engineering in recent years. But the ground disturbance induced by the quasirectangular tunneling needs further researches. This paper derives the calculation formula of the additional stress of existing shield tunnel below caused by the quasirectangular shield tunneling by mirror image method and Mindlin solution. The existing shield tunnel is simplified as an elastic foundation short beam connected by tensile springs and shear springs. This paper establishes the energy-deformation coupling equation by principle of minimum potential energy so that the disturbance induced by quasirectangular tunneling to the existing shield tunnel below can be analyzed. The FEM is established with the actual engineering as the background. It is by comparing the numerical simulation results and field monitoring data that the theoretical prediction formula is verified. The research results show that the theoretical calculation results consist highly with numerical simulation results and field monitoring data, verifying practicality of formulas in this paper. Calculation results of shear stagger model are more accurate, which can be also used to analyze the staggered and splayed amount between segments. As the tunnel construction proceeds, uplift deformation, segment stagger, shear force, and segment splay of existing shield tunnel gradually increase, which are symmetrical about the central axis of new tunnel. After the shield machine passes through the central axis of the existing shield tunnel for 20 meters, stable disturbance to the existing shield tunnel occurs. Stagger amount and shear force between segments reach the minimum at the position with maximum uplift deformation of existing shield tunnel and reach the maximum at inflection point of the uplift deformation curve.

1. Introduction

Two roughly parallel circular tunnels need to be built for each line so as to meet the demand for two-way operation of trains. The construction of two tunnels for one line does not only occupy more underground space and increase the construction cost, but also the necessary distance between the two tunnels is within the scope of the subway protection zone, which cannot be developed and utilized, resulting in low utilization of underground space. Improving effective utilization of underground space, Japan has successively developed special-shaped shield technology since the 1970s, such as rectangular shield and double-circle shield. The quasirectangular shield tunnel has advantage of high utilization rate of tunnel section. It can accommodate the two-way passage of trains by only one tunnel for each line, which greatly saves the construction cost and makes full use of the limited urban underground space, and has significant economic and social benefits [1–3]. With the further improvement of quasirectangular shield construction method, those tunnels would have a wide range of application prospects. The underground space in the city is extremely limited, and the underground lines often overlap up and down. As a result, it is practically significant to carry out the research on the disturbance to existing shield tunnel below by quasirectangular shield tunneling.

Research methods for the disturbance of surrounding lines by tunnel construction include theoretical analysis method, numerical simulation method, and model experiment method [4–6]. Wu et al. [7] use 3D discrete element

method to study the influence of new tunnel construction on existing shield tunnel and propose a method to reduce disturbance to the existing shield tunnel; Wu et al. [8] consider factors such as different excavation sequences for new tunnel, stratum loss, and gap between old and new tunnels. Indoor centrifugal tests and 3D numerical analysis are developed to study the impact mechanism of overcrossing tunnels on existing shield tunnel; Lai et al. [9] present a special case study where the new tunnel was built at an incline near the existing shield tunnel above, with a small crossing angle. The settlement characteristics of existing shield tunnel are studied by monitoring data and finite difference method (FDM) numerical simulations; Deng et al. [10] propose a ground damage model for shield tunnel construction along these sections. Ground surface subsidence prediction formula is derived using mirror image theory and Mindlin solution; Vorster et al. [11] develop a finite element model to study a tunnel passing vertically beneath an existing shield tunnel; Zhang et al. [12] propose an analytical solution to study response of existing shield tunnel induced by the excavation of new tunnels. Timoshenko beams on the Kerr foundation are used to simulate ground disturbances in existing shield tunnel caused by the new shield tunneling. To sum up, there are few researches on the construction of new tunnel crossing over existing shield tunnel, and most researches study the new shield tunnels with circular cross-section. New quasirectangular shield tunnels differ from the circular shield tunnels in the shield front thrust, shield shell friction, and grouting pressure distribution forms due to the complex cross-section convergence. There is currently no specific calculation model. Therefore, it is very meaningful to consider the factors of quasirectangular shield tunnel excavation, establish a reasonable mechanical calculation model and prediction formula, and analyze the disturbance of quasirectangular shield tunnel construction to the existing shield tunnel below.

The main contents of this study include the following: Firstly, the mechanical model of tunneling calculation of the quasirectangular shield tunnel is established. Additional stress derived by the stratum loss, the front thrust of shield, the friction force of shield shell, and the grouting pressure at shield tail during the tunneling process of the quasirectangular shield is calculated by using the mirror image method and the Mindlin solution. Then, the shear stagger model and the minimum potential energy principle are adapted to calculate vertical deformation of existing shield tunnel below, segment stagger, and shear force, which all changes with the tunneling distance of the shield machine. Taking a subway project in Ningbo as the background, this paper establishes a numerical calculation model, compared with the theoretical prediction results, and on-site monitoring data and verifies rationality of theoretical model and prediction formula. This study can provide theoretical guidance for similar engineering.

2. Theoretical Computational Assumptions

The main factors that disturb the surrounding strata during the shield tunneling include the stratum loss, the front thrust of shield, the friction force of shield shell, and the grouting pressure at shield tail. This paper calculates the combined effect of the factors above to obtain deformation and mechanical characteristics of existing shield tunnel. The following is assumed in the calculation:

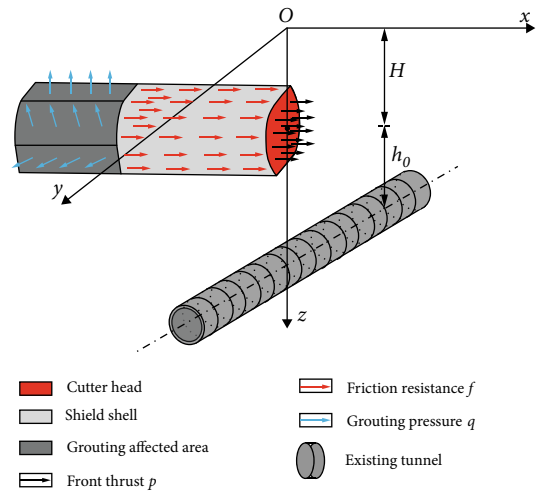

Figure 1: Diagram of construction calculation for quasirectangular shield tunnel.

(1) Stratum is a homogeneous linear elastic semi-infinite body, and the effect of stratum stratification is not considered. Transform different stratum with different properties into homogeneous single-property stratum by the equivalent stratum method [13]

(2) The quasirectangular shield machine drives along a straight line, regardless of the offset of the shield machine during the excavation

(3) Stratum consolidation and grouting slurry solidification are not considered, while the effect of load on stratum is considered. The frontal thrust of shield is evenly distributed on the cutter, the frictional resistance of shield shell is evenly distributed on surface of shield shell, and grouting pressure is evenly distributed on the surface of last 3 segments of the shield tail

According to the existing research and assumptions above, the calculation model of the overcrossing construction of new tunnel is established as shown in Figure 1. In the figure, the shield cutter is located on the yoz plane, the x-axis represents longitudinal distance from calculation point to center point of shield machine, the y-axis represents lateral distance of that, and the z-axis represents depth of the calculation point. Coordinates of centerline point of the cutter are $(0, 0, H)$, and the distance from the existing shield tunnel to quasirectangular tunnel is h_0 . p represents the front thrust of shield, f represents the friction force of shield shell, and q represents grouting pressure at shield tail.

3. Additional Stress due to Stratum Loss

3.1. The Basic Principle of Mirror Image Method. Sagaseta [14] proposed the mirror image method, assuming that stratum is an infinite body, and the stress generated in the stratum by a void with a radius of a at the underground (x_0, y_0, z_0) is composed of three parts: (1) The true action point of application induces the normal stress σ_0 and shear stress τ_0 of the infinite body. (2) The mirror action point above the ground induces stress in the infinite body and on the ground. (3) It is assumed that a tangential stress on the ground which is opposite to τ_0 and twice its size generates stress field at each point below the ground.

It can be calculated that the additional stress of the first part and the second part generated by the real action point and the mirror action point at a certain underground point (ξ, η, ε) can be expressed as follows:

$$\begin{aligned}
\sigma_{x1-2} &= a^3\frac{E}{3(1-2\mu)}\left(\frac{1}{r_2^3}-\frac{1}{r_1^3}\right)+a^3\frac{E(1-\mu)}{(1-2\mu)(1+\mu)}\cdot(\xi-x_0)^2\left(\frac{1}{r_1^5}-\frac{1}{r_2^5}\right)+a^3\frac{E\mu}{(1-2\mu)(1+\mu)}\cdot\left[(\eta-y_0)^2\left(\frac{1}{r_1^5}-\frac{1}{r_2^5}\right)+(\varepsilon-z_0)^2\frac{1}{r_1^5}-(\varepsilon+z_0)^2\frac{1}{r_2^5}\right],\\
\sigma_{y1-2} &= a^3\frac{E}{3(1-2\mu)}\left(\frac{1}{r_2^3}-\frac{1}{r_1^3}\right)+a^3\frac{E(1-\mu)}{(1-2\mu)(1+\mu)}\cdot(\eta-y_0)^2\left(\frac{1}{r_1^5}-\frac{1}{r_2^5}\right)+a^3\frac{E\mu}{(1-2\mu)(1+\mu)}\cdot\left[(\xi-x_0)^2\left(\frac{1}{r_1^5}-\frac{1}{r_2^5}\right)+(\varepsilon-z_0)^2\frac{1}{r_1^5}-(\varepsilon+z_0)^2\frac{1}{r_2^5}\right],\\
\sigma_{z1-2} &= a^3\frac{E}{3(1-2\mu)}\left(\frac{1}{r_2^3}-\frac{1}{r_1^3}\right)+a^3\frac{E(1-\mu)}{(1-2\mu)(1+\mu)}\cdot\left[\frac{(\varepsilon-z_0)^2}{r_1^5}-\frac{(\varepsilon+z_0)^2}{r_2^5}\right]+a^3\frac{E\mu}{(1-2\mu)(1+\mu)}\cdot\left[(\xi-x_0)^2+(\eta-y_0)^2\right]\cdot\left(\frac{1}{r_1^5}-\frac{1}{r_2^5}\right),
\end{aligned} \tag{1}$$

where r_1 and r_2 are as follows:

$$\begin{aligned}
r_1 &= \sqrt{(\xi-x_0)^2+(\eta-y_0)^2+(\varepsilon-z_0)^2},\\
r_2 &= \sqrt{(\xi-x_0)^2+(\eta-y_0)^2+(\varepsilon+z_0)^2}.
\end{aligned} \tag{2}$$

The third part of the additional stress generated by the tangential stress at the surface at a certain point (ξ, η, ε) underground can be expressed as follows:

$$\begin{aligned}
\sigma_{x3} &= \frac{a^3}{\pi}\frac{E}{1+\mu}\lim_{b\to\infty}\lim_{c\to\infty}\int_{y_0-b}^{y_0+b}\int_{x_0-c}^{x_0+c} z_0\frac{(\xi-u)(u-x_0)}{\left[(u-x_0)^2+(t-y_0)^2+z_0^2\right]^{5/2}}\\
&\quad\times\left\{\frac{1-2\mu}{(R+\varepsilon)^2}\times\left[\frac{1}{R}-\frac{(\eta-t)^2}{R^3}-\frac{2(\eta-t)^2}{R^2(R+z)}\right]-\frac{3(\xi-u)^2}{R^5}\right\}\mathrm{dudt}\\
&\quad+\frac{a^3}{\pi}\frac{E}{1+\mu}\lim_{b\to\infty}\lim_{c\to\infty}\int_{y_0-b}^{y_0+b}\int_{x_0-c}^{x_0+c} z_0\frac{(\eta-t)(t-y_0)}{\left[(u-x_0)^2+(t-y_0)^2+z_0^2\right]^{5/2}}\\
&\quad\times\left\{\frac{1-2\mu}{(R+\varepsilon)^2}\times\left[\frac{1}{R}-\frac{(\xi-u)^2}{R^3}-\frac{2(\xi-u)^2}{R^2(R+\varepsilon)}\right]-\frac{3(\eta-t)^2}{R^5}\right\}\mathrm{dudt},\\
\sigma_{y3} &= \frac{a^3}{\pi}\frac{E}{1+\mu}\lim_{b\to\infty}\lim_{c\to\infty}\int_{y_0-b}^{y_0+b}\int_{x_0-c}^{x_0+c} z_0\frac{(\xi-u)(u-x_0)}{\left[(u-x_0)^2+(t-y_0)^2+z_0^2\right]^{5/2}}\\
&\quad\times\left\{\frac{1-2\mu}{(R+\varepsilon)^2}\times\left[\frac{1}{R}-\frac{(\xi-u)^2}{R^3}-\frac{2(\xi-u)^2}{R^2(R+\varepsilon)}\right]-\frac{3(\eta-t)^2}{R^5}\right\}\mathrm{dudt}\\
&\quad+\frac{a^3}{\pi}\frac{E}{1+\mu}\lim_{b\to\infty}\lim_{c\to\infty}\int_{y_0-b}^{y_0+b}\int_{x_0-c}^{x_0+c} z_0(\eta-t)(t-y_0)\left[(u-x_0)^2+(t-y_0)^2+z_0^2\right]^{5/2}\\
&\quad\times\left\{\frac{1-2\mu}{(R+\varepsilon)^2}\times\left[\frac{1}{R}-\frac{(\eta-t)^2}{R^3}-\frac{2(\eta-t)^2}{R^2(R+\varepsilon)}\right]-\frac{3(\xi-u)^2}{R^5}\right\}\mathrm{dudt}.\\
\sigma_{z3} &= \frac{a^3}{\pi}\frac{3E}{1+\mu}\lim_{b\to\infty}\lim_{c\to\infty}\int_{y_0-b}^{y_0+b}\int_{x_0-c}^{x_0+c}\varepsilon^2 z_0\frac{(\xi-u)(u-x_0)}{\left[(u-x_0)^2+(t-y_0)^2+z_0^2\right]^{5/2}}\frac{1}{R^5}\mathrm{dudt}\\
&\quad+\frac{a^3}{\pi}\frac{3E}{1+\mu}\lim_{b\to\infty}\lim_{c\to\infty}\int_{y_0-b}^{y_0+b}\int_{x_0-c}^{x_0+c}\varepsilon^2 z_0\frac{(\eta-t)(t-y_0)}{\left[(u-x_0)^2+(t-y_0)^2+z_0^2\right]^{5/2}}\frac{1}{R^5}\mathrm{dudt},
\end{aligned} \tag{3}$$

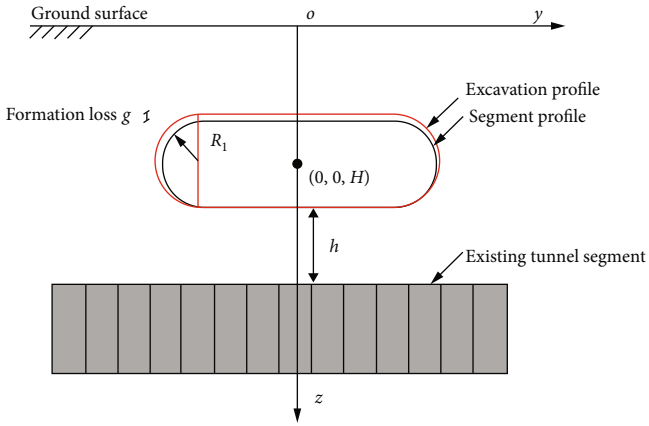

Figure 2: The calculation diagram of additional stress caused by stratum loss.

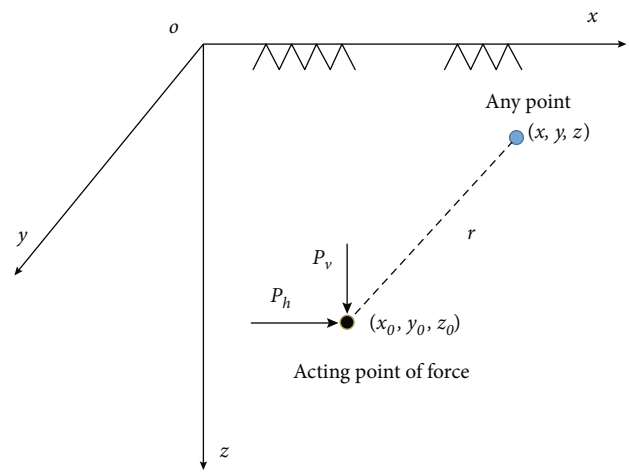

Figure 3: Mindlin solution calculation diagram.

where E is the elastic modulus of stratum. μ is the Poisson's ratio.$R = [(\xi - \mu)^2 + (\eta - t)^2 + \varepsilon^2]^{1/2}$.

It can be obtained by the superposition of stratum additional stress calculated above: total additional stress generated at the point (ξ, η, ε) by the void with radius a at (x_0, y_0, z_0) in the semi-infinite stratum body is

$$\sigma_i = \sigma_{i1-2} + \sigma_{i3}. \tag{4}$$

The additional stress generated by the unit volume void is

$$\sigma_i' = \frac{\sigma_i}{(4\pi a^3/3)}, \tag{5}$$

where $i = x, y, z$.

3.2. Calculation of Additional Stress Induced by Stratum Loss. The diameter of shield shell is larger than that of segment lining while shield tunneling. However, there is still a gap between the segments and stratum after shield tail comes out, which is generally filled by grouting in engineering. However, due to the time required for grouting slurry to solidify and the volume reduction after grouting solidifies, there is a certain amount of stratum loss within the shield tail segments. It is assumed that the displacement mode of the stratum during the quasirectangular shield tunneling is nonequivalent radial movement of tunnel subsidence, as shown in Figure 2. In calculation process, excavation surface is simplified to consist of two semicircles on the left and right and a rectangle in the middle. H is the depth of centerline of quasirectangular tunnel. h is the depth of the existing shield tunnel centerline. h_0 is the distance between two tunnels. d is the width of long side of the rectangle in excavation face of quasirectangular tunnel.

The volume of stratum loss can be regarded as the gap between two tangent quasirectangular bodies inside and outside, and the length of the quasirectangular body is l. The volume of stratum loss can be written as $V = V_{R_2} - V_{R_1}$.

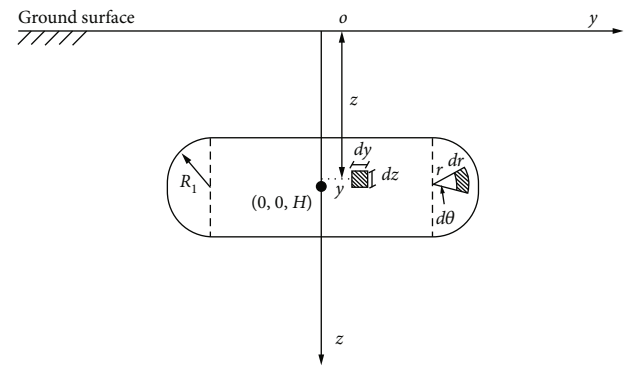

Figure 4: The calculation diagram of additional stress caused by front thrust of shield.

V_{R_2} is the volume of the outside quasirectangular body, $V_{R_2} = l(\pi R_2^2 + 4dR_2)$. R_2 is the radius of the outer circle. V_{R_1} is the volume of the inside quasirectangular body, $V_{R_1} = l(\pi R_1^2 + 4dR_1)$. R_1 is the radius of the inner circle.

By integrating the additional stress generated by the unit volume void at the existing shield tunnel axis, the vertical additional stress generated by the stratum loss at the existing shield tunnel axis can be obtained:

$$\sigma_{zloss} = \iiint_{V_{R_2} - V_{R_1}} \sigma_z' dxdydz. \tag{6}$$

4. Additional Stress Caused by Shield Construction

4.1. Mindlin Additional Stress Solution. In the elastic infinite homogeneous body, the Mindlin solution [15] can be used to calculate the additional stress generated during shield tunneling process. The calculation diagram is shown in Figure 3. In a homogeneous elastic infinite body (x_0, y_0, z_0), a horizontal force P_h and a vertical force P_v act, and the vertical additional stress generated by the acting force at

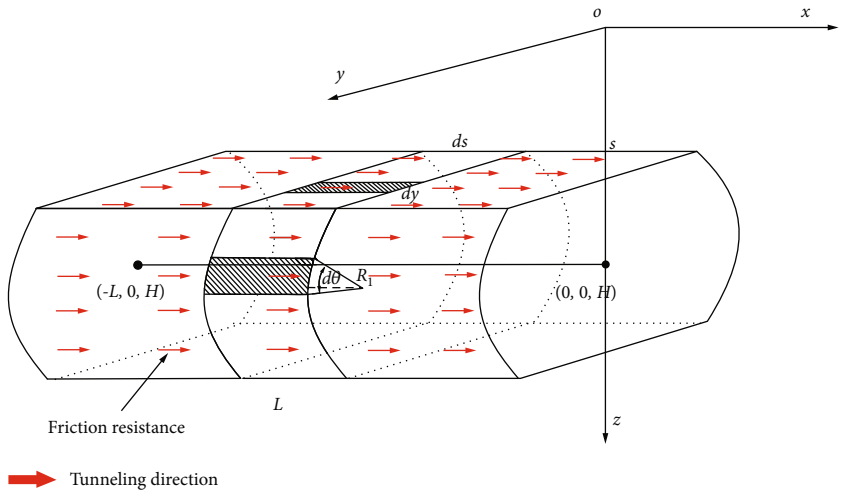

Figure 5: The calculation diagram of additional stress induced by shield friction.

any point (ξ, η, ε) in the infinite body is

$$\sigma_z^1 = -\frac{p_h}{8\pi(1-\mu)}\left\{\frac{1-2\mu}{R_1^3} - \frac{1-2\mu}{R_2^3} - \frac{3(\varepsilon-z_0)^2}{R_1^5} - \frac{3(3-4\mu)(\varepsilon+z_0)^2}{R_2^5} + \frac{6z_0}{R_2^5}\left[z_0 + (1-2\mu)\times(\varepsilon+z_0) + \frac{5\varepsilon(\varepsilon+z_0)^2}{R_2^2}\right]\right\}, \tag{7}$$

$$\sigma_z^2 = -\frac{p_v}{8\pi(1-\mu)}\left[-\frac{(1-2\mu)(\varepsilon-z_0)}{R_1^3} + \frac{(1-2\mu)(\varepsilon-z_0)}{R_2^3} - \frac{3(\varepsilon-z_0)^3}{R_1^5} - \frac{3(3-4\mu)\varepsilon(\varepsilon+z_0)^2}{R_2^5} + \frac{3z_0(\varepsilon+z_0)(5\varepsilon-z_0)}{R_2^5} - \frac{30(\varepsilon-z_0)\varepsilon(\varepsilon+z_0)^3}{R_2^7}\right], \tag{8}$$

where R_1 and R_2 are as follows:

$$R_1 = \sqrt{(\xi-x_0)^2 + (\eta-y_0)^2 + (\varepsilon-z_0)^2},$$
$$R_2 = \sqrt{(\xi-x_0)^2 + (\eta-y_0)^2 + (\varepsilon+z_0)^2}. \tag{9}$$

4.2. Additional Stress Caused by Frontal Thrust of Shield. Tunnel face is shown in Figure 4, which is simplified to consist of two semicircles and a rectangle in the middle. Taking any element $dA_1 = r_1 dr d\theta$ on the two semicircles, the frontal thrust on the element is $dF_{p1} = p r dr d\theta$. Taking any element $dA_2 = dxdy$ in the rectangular part, the frontal thrust on the element is $dF_{p2} = pdxdz$. The center coordinates of the tunnel face are $(0, 0, H)$. Substitute dF_{pi} into Equation (7) to integrate the tunnel face for vertical additional stress σ_{zp}^1 generated at axis of existing shield tunnel. Element coordinates need to be transformed during the integration process:

$$\text{semicircle part}: \begin{cases} x_0 = d + r\cos\theta (\text{the right part of the tunnel face}), \\ -d + r\cos\theta (\text{the left part of the tunnel face}), \\ y_0 = 0, \\ z_0 = H - r\sin\theta, \end{cases}$$
$$\text{rectangular part}: \begin{cases} x_0 = x, \\ y_0 = 0, \\ z_0 = z. \end{cases} \tag{10}$$

The additional stress induced by the frontal thrust of shield at the existing shield tunnel axis (ξ, η, ε) can be expressed as follows:

$$\sigma_{zp}^1 = \int_0^{R_1}\int_{-\pi/2}^{\pi/2}\sigma_z^1 dr d\theta + \int_0^{R_1}\int_{\pi/2}^{3\pi/2}\sigma_z^1 dr d\theta + \int_{H-R_1}^{H+R_1}\int_{-d}^{d}\sigma_z^1 dx dz. \tag{11}$$

4.3. Additional Stress Induced by Shield Friction. While shield tunneling, the friction force generated by contact between the shield and the surrounding stratum will affect the displacement of the stratum. The calculation diagram of additional stress induced by friction of shield shell is shown in Figure 5, where s is the horizontal distance between the integral unit and the cutter and L is the length of shield. Taking any unit $dA_1 = R_1 ds d\theta$ on the two semicircles, the shield friction force on the unit is $dF_{f1} = f R_1 ds d\theta$. Taking any unit $dA_2 = dxdy$ in the rectangular part, the shield friction force on the unit is $dF_{f2} = fdxdy$. Substitute dF_{fi} into Equation (8) and integrate within the shield shell range to obtain the vertical additional stress induced by shield shell friction force σ_{2f}^1 at axis of existing shield tunnel. The element coordinates need to be transformed during the

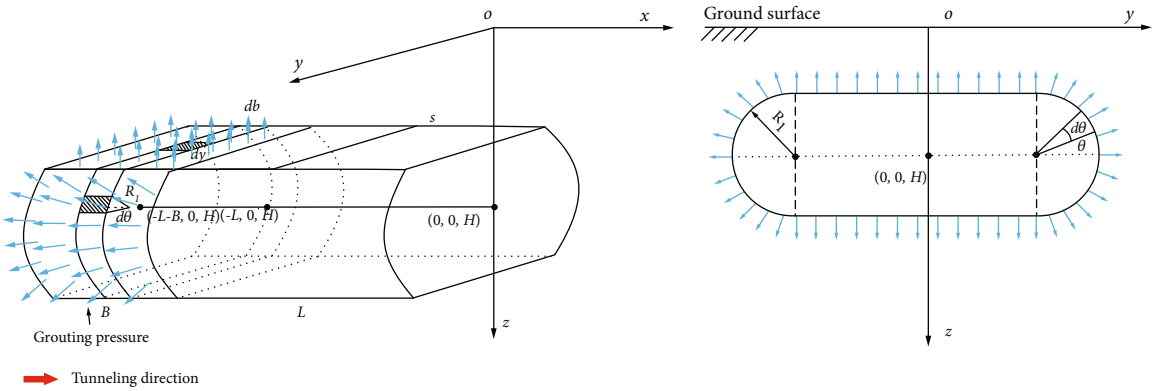

(a) 3D distribution of grouting pressure

(b) Grouting pressure plane distribution

Figure 6: The calculation diagram of additional stress caused by grouting pressure at shield tail.

integration process:

$$\text{semicircle part}: \begin{cases} x_0 = d + R_1 \cos\theta (\text{the right part segment of shield shell}), \\ -d + R_1 \cos\theta (\text{the left part segment of shield shell}), \\ y_0 = -s, \\ z_0 = H - R_1 \sin\theta, \end{cases}$$

$$\text{rectangular part}: \begin{cases} x_0 = x, \\ y_0 = y, \\ z_0 = H - R_1 (\text{upper part of shield segment}), \\ z_0 = H + R_1 (\text{lower part of shield segment}). \end{cases} \tag{12}$$

The additional stress induced by shield friction at the existing shield tunnel axis (ξ, η, ε) can be expressed as follows:

$$\sigma_{zf}^1 = \int_0^L \int_{-\pi/2}^{\pi/2} \sigma_z^1 \mathrm{d}s\mathrm{d}\theta + \int_0^L \int_{\pi/2}^{3\pi/2} \sigma_z^1 \mathrm{d}s\mathrm{d}\theta + \int_0^L \int_{-d}^{d} \sigma_z^1 \mathrm{d}x\mathrm{d}y. \tag{13}$$

4.4. Additional Stress Induced by Grouting Pressure at Shield Tail. Calculation diagram of additional stress induced by grouting pressure q at shield tail is shown in Figure 6, and the length of the shield tail segment is a. It can be obtained that grouting pressure at the semicircular part is distributed radially along the cross-section, which is decomposed into the horizontal grouting pressure $q_x = q\cos\theta$ and the vertical grouting pressure $q_z = q\sin\theta$. Taking any unit $\mathrm{dA}_1 = \mathrm{R}_1 \mathrm{dsd}\theta$ at the semicircular parts of shield tail, horizontal grouting pressure and vertical grouting pressure received by this unit are $\mathrm{dF}_{qx} = q\cos\theta \mathrm{R}_1 \mathrm{dsd}\theta$ and $\mathrm{dF}_{qz} = q\sin\theta \mathrm{R}_1 \mathrm{dsd}\theta$, respectively. Taking any unit $\mathrm{dA} = \mathrm{dxdy}$ at the rectangular grouting part of shield tail, the grouting pressure of this unit is $\mathrm{dF}_q = \mathrm{qdxdy}$. Substitute dF_{qx} into Equation (7) and dF_q and dF_{qz} into Equation (8), and integrate within the shield tail grouting range to obtain the vertical additional stress generated by grouting pressure at existing shield tunnel axis. The element coordinates need to be transformed during the integration process:

$$\text{semicircle part}: \begin{cases} x_0 = d + R_1 \cos\theta (\text{the right part of segment at shield tail}), \\ -d + R_1 \cos\theta (\text{the left part of segment at shield tail}), \\ y_0 = -s, \\ z_0 = H - R_1 \sin\theta, \end{cases}$$

$$\text{rectangular part}: \begin{cases} x_0 = x, \\ y_0 = y, \\ z_0 = H - R_1 (\text{upper part of shield segment}), \\ z_0 = H + R_1 (\text{lower part of shield segment}). \end{cases} \tag{14}$$

Additional stress generated by shield tail grouting pressure at the existing shield tunnel axis (ξ, η, ε) can be expressed as follows:

$$\begin{aligned} \sigma_{zq}^1 &= \int_L^{L+a} \int_{-\pi/2}^{\pi/2} \sigma_z^1 \mathrm{d}s\mathrm{d}\theta + \int_L^{L+a} \int_{\pi/2}^{3\pi/2} \sigma_z^1 \mathrm{d}s\mathrm{d}\theta, \\ \sigma_{zq}^2 &= \int_L^{L+a} \int_{-\pi/2}^{\pi/2} \sigma_z^2 \mathrm{d}s\mathrm{d}\theta + \int_L^{L+a} \int_{\pi/2}^{3\pi/2} \sigma_z^2 \mathrm{d}s\mathrm{d}\theta + \int_L^{L+a} \int_{-d}^{d} \sigma_z^2 \mathrm{d}x\mathrm{d}y. \end{aligned} \tag{15}$$

To sum up, by superimposing additional stress generated by the stratum loss, front thrust of shield, friction force of shield shell, and grouting pressure at shield tail at axis of existing shield tunnel, during the excavation process of the quasirectangular shield, the additional stress σ_z at axis of existing shield tunnel can be expressed as follows:

$$\sigma_z = \sigma_{\mathrm{zloss}} + \sigma_{zp}^1 + \sigma_{zf}^1 + \sigma_{zq}^1 + \sigma_{zq}^2. \tag{16}$$

5. Calculation of Vertical Deformation of Tunnel

5.1. Shear Stagger Model. Wu et al. [8] proposed a shear stagger model, regarding segments as a short beam of elastic foundation connected by tensile springs and shearing springs. Considering rigid body rotation effect and shear

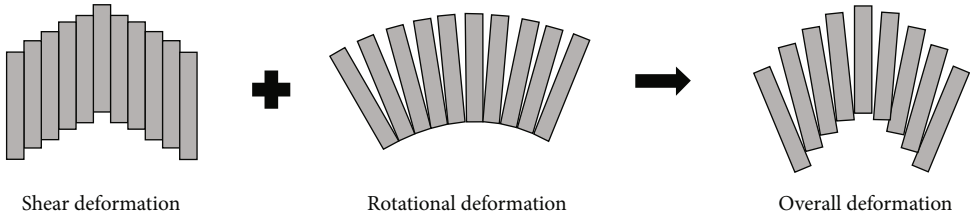

Figure 7: Shear stagger model.

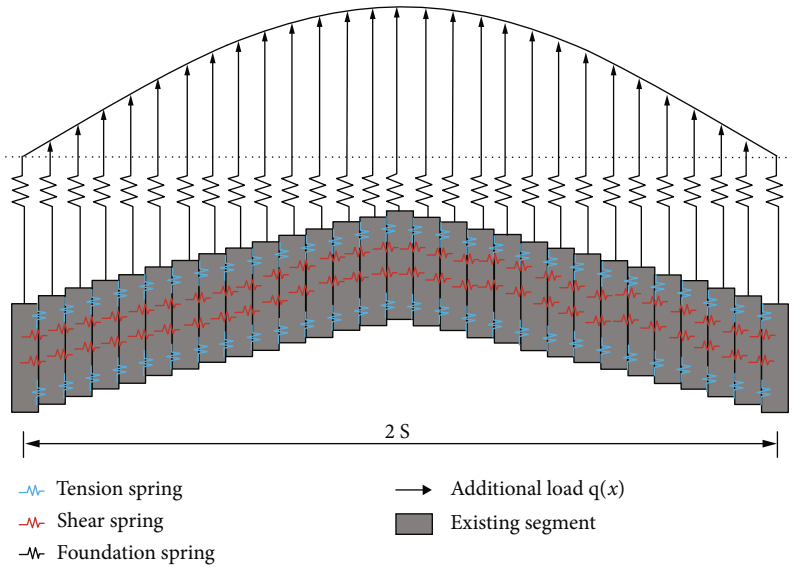

Figure 8: Calculation model of shearing stagger of existing shield tunnel.

stagger effect comprehensively, the tunnel deformation is regarded as rigid body rotation on the basis of shear stagger, as shown in Figure 7.

There will be both relative rotation angle and relative stagger displacement between adjacent segments. Tunnel's longitudinal deformation of the tunnel is formed by combination of shear stagger and rigid body rotation between adjacent segments. When the total relative vertical displacement between adjacent segments is δ, the relative vertical displacement caused by rigid body rotation of segments is δ_1, and the relative vertical displacement caused by stagger of segment rings is δ_2, and it can be expressed as $\delta = \delta_1 + \delta_2$. Let $\delta_1 = i\delta$, and j is proportional coefficient of rigid body rotation effect of the segment, which represents ratio of relative vertical displacement caused by the rigid body rotation between adjacent segments to the total relative vertical displacement.

5.2. Total Potential Energy of Existing Tunnel. Deformation of existing shield tunnel is simulated by shear stagger model. In the calculation process, it is assumed that the affected area by new tunnel construction is 2*S*. Existing shield tunnel segment in 2*S* unit is regarded as the elastic foundation short beam connected with shearing spring and the tensile spring. The overcrossing new tunnel causes the deformation of existing shield tunnel in the way of shear stagger between segments, as shown in Figure 8.

An existing shield tunnel segment with a width of w is selected for force analysis, and the deformation and force conditions are shown in Figure 9.

Vertical load F_z on the segment can be expressed as

$$F_z = P_z(x) - \mathrm{kDS}_z(x) - k_t[w_z((m+1)\omega) - w_z(m\omega)] - \frac{1}{2}k_t[w_z(m\omega) - ((m-1)\omega)]. \quad (17)$$

In the formula, $P_z(x)$ is the additional load generated by quasirectangular shield tunneling, $P_z(x) = D\sigma_z$. D is diameter of existing shield tunnel. k is foundation bed coefficient, which is calculated by reference [16–18]; $k = 1.3E_S{}^{12}\sqrt{E_S D^4/E_t I_t[D(1-\mu^2)]}$. E_S is elastic modulus of foundation stratum, and $E_t I_t$ is equivalent bending stiffness of tunnel. k_t is circumferential shear stiffness of the tunnel [19–21]. $S_Z(x)$ is the displacement of the foundation spring, according to the displacement coordination condition, $S_z(x) = W_z(x)$, and $W_z(x)$ represents the horizontal displacement of existing shield tunnel.

Total potential energy of existing shield tunnel can be divided into three parts: (1) The additional stress acts W^p generated by new shield tunneling at axis of existing shield tunnel. (2) Existing shield tunnel is placed on elastic foundation and overcomes elastic resistance to act W^k during the deformation process. (3) Existing shield tunnel overcomes

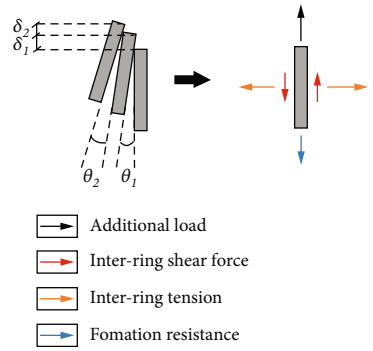

Figure 9: The stress of single segment.

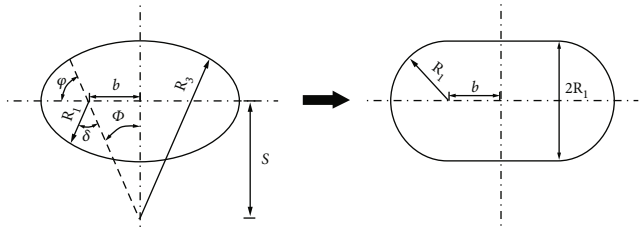

Figure 10: Cross-section of quasirectangular shield tunnel and equivalent interface.

Table 1: The geometric dimensions of quasirectangular shield tunnel.

Small circle radius R_1 (m)	Great circle radius R_3 (m)	Long side of rectangle b (m)	Offset S (m)	φ (°)	δ (°)	ψ (°)
3.37	15.61	2.55	11.97	78	24	12

the shear resistance between segments to act W^s. Total potential energy of existing shield tunnel is

$$E^p = W^P + W^k + W^s. \tag{18}$$

5.3. Displacement Function of Existing Shield Tunnel. Lu et al. [22] proposed a unified displacement function that uses a Fourier series to represent tunnel. Unified displacement function is expanded according to Fourier series:

$$W_z = \sum_{n=0}^{\infty} a_n \cos\frac{n\pi x}{N\omega} = \{T_n(x)\}\{A\}, \tag{19}$$

where $T_n(x) = \{1, \cos(\pi x/N\omega), \cos(2\pi x/N\omega), \cdots, \cos(n\pi x/N\omega),\}$, $A = \{a_0, a_1, a_2, \cdots, a_n\}$ is the undetermined coefficient, and n is expansion order of Fourier series.

5.4. Variational Governing Equations. By principle of minimum potential energy, taking total potential energy E^p of existing shield tunnel to extreme value of each undetermined coefficient, it can be obtained as

$$\frac{\partial E^p}{\partial a_i} = 0 (i = 0, 1, 2, \cdots, n), \tag{20}$$

where a_i is an element in matrix A.

After solving Equation (20), the control equation of vertical displacement of existing shield tunnel is obtained as

$$\left\{\sum_{m=-N}^{N-1}\frac{\partial[w_z((m+1)\omega) - w_z(m\omega)]}{\partial a_i}[T_n((m+1)\omega) - T_n(m\omega)]\right\} + \int_{-N\omega}^{N\omega} -\mathrm{kD}\frac{\partial w_z(x)}{\partial a_i}\{T_n(x)\}\mathrm{dx}\cdot\{A\} = \int_{-N\omega}^{N\omega} P_z(x)\{T_n(x)\}^T\mathrm{dx}. \tag{21}$$

In the formula, $2N$ is the number of segments of the existing shield tunnel affected by the new tunnel. Express Equation (21) in matrix form:

$$([K_t] + [K_s])\{A\} = \{P_z\}^T. \tag{22}$$

In the formula, $[K_t]$ is stiffness matrix between segments, and $[K_s]$ is stratum stiffness matrix, respectively, expressed as

$$[K_t] = \sum_{m=-N}^{N-1} k_t\left[T_n((m+1)\omega)^T - T_n(m\omega)^T\right]\times[T_n((m+1)\omega) - T_n(m\omega)],$$
$$[K_s] = \mathrm{kDS}\begin{bmatrix} 2 & & & \\ & 1 & & \\ & & \ddots & \\ & & & 1 \end{bmatrix}. \tag{23}$$

$\{P_z\}^T$ represents interaction effect between the segments and the free stratum displacement, which can be expressed as

$$\{P_z\}^T = \int_{-N\omega}^{N\omega} P_z(x)\{T_n(x)\}^T\mathrm{dx}. \tag{24}$$

$\{A\}$ is obtained from Equation (22), substituted into Equation (19) to obtain vertical displacement of existing shield tunnel affected by quasirectangular shield tunneling. The stagger amount between adjacent segments is specifically expressed as

$$\Delta W_z = w_z((m+1)\omega) - w_z(m\omega). \tag{25}$$

The shear force between adjacent segments is specifically expressed as

$$Q_z = k_t \times [w_z((m+1)\omega) - w_z(m\omega)]. \tag{26}$$

The above algorithm is numerically calculated by MATLAB programming, and existing shield tunnel segment stiffness matrix $[K_t]$ and stratum stiffness matrix $[K_s]$ can be

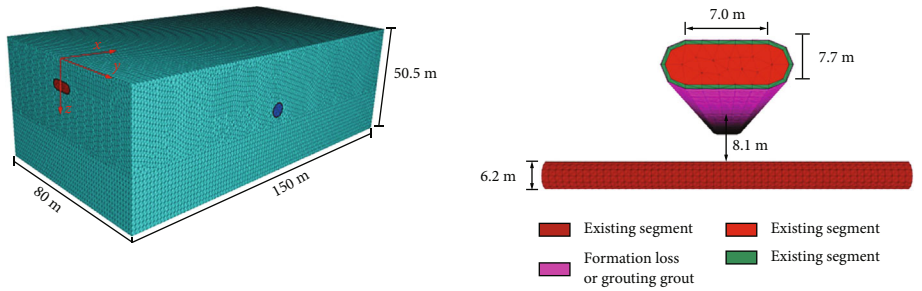

(a) Overall model (b) Rectangular-like tunnels and existing shield tunnel

Figure 11: Numerical computation model.

Table 2: Physical and mechanical parameters of stratum.

Bulk density γ (kN·m^{-3})	Cohesion force c (kPa)	Internal friction angle ϕ (°)	Compression modulus E_s (MPa)	Poisson's ratio μ
18	10.5	14.45	7.46	0.32

taken as 10th order to meet requirements of engineering accuracy.

6. Numerical Simulation Model

6.1. Engineering Background. Ningbo Railway Line 3 is the first test section in China that uses a quasirectangular shield tunnel, whose section in this route used in the calculation is as shown in Figure 10. The size parameters of new shield tunnel are shown in Table 1.

The shape of the quasirectangular section is actually complex. In order to simplify the calculation, this paper simplifies its section into a rectangle and two semicircles without changing its basic geometric dimensions of the length, width, and height, as shown in Figure 11. In the figure, the radius of excavation face $R_1 = 3.37$ m, the long side of the rectangle $d = 3.5$ m, the depth of the tunnel center $h = 13.07$ m, and the stratum loss gap parameter $g = 42$ mm. It is analyzed that simplified calculation model has little error with actual size, satisfying demand for engineering accuracy.

6.2. Modelling and Materials. According to simplified quasirectangular tunnel face, FEM is established, shown in Figure 11. Distance from buried depth of existing shield tunnel to the central axis of new shield tunnel is $h_0 = 8.1$ m. Buried depth H of new shield tunnel is 8 m. Reducing influence of boundary conditions on model calculation, distance from the model boundary to the new quasirectangular tunnel needs to be greater than three times the tunnel diameter to simulate the excavation of shield, so that model size is taken as $80 \times 100 \times 50.5$ m. The material types in this model mainly include stratum, existing shield tunnel, new tunnel segments, shield cutter, and shield shells. The Mohr-Coulomb constitutive model is used for stratum, and linear elastic constitutive model is used for the rest of the materials. According to the on-site survey data and the equivalent stratum method, physical and mechanical parameters of stratum around tunnel are shown in Table 2.

Other material parameters obtained from the design and construction report are shown in Table 3.

6.3. Model Boundaries and Calculation Steps. Before the calculation, it is necessary to impose boundary conditions on model: displacement of bottom surface is fixed, upper surface is free with deformation, and the normal deformation of the other four horizontal surfaces is constrained. The model calculation follows the following steps:

Step 1: remove stratum of existing shield tunnel in lower part, assign elastic material to tunnel segment, and calculate displacement and stress after shield tunneling

Step 2: set displacement field in step 1 to zero and keep the stress field. The new tunnel starts to be excavated at a distance of 50 m ($y = 50$ m) from existing shield tunnel axis, and total excavation distance is 100 m ($y = -50$ m). When new tunnel is excavated for 50 m ($y = 0$ m), the axes of the two tunnels are orthogonal. Gradually remove the stratum in shield shell of new quasirectangular tunnel, assign material parameters corresponding to the shield cutter, shield shell, and segment, and assign the shield tail gap to the Null element. According to the actual situation on site, the additional shield thrust is 20 kPa, the average value of shield friction is 18 kPa, and the grouting pressure is 25 kPa. Excavation is carried out step by step and the corresponding loads are applied, and disturbance of existing shield tunnel below is calculated

6.4. Analysis of Calculation Results

6.4.1. Ground Surface Deformation Analysis. Figure 12 is the cloud map of ground surface subsidence when it is excavated to 75 m. Ground surface subsidence cloud map is symmetrically distributed, and the maximum subsidence position is located above new tunnel, and the maximum subsidence is 37.1 cm. The effect of the stratum pressure above causes the deformation of quasirectangular tunnel, and deformation of segment spreads to the periphery, causing the stratum to settle. Due to unloading of the excavated stratum, uplift deformation occurs under the new rectangular tunnel, and the maximum uplift deformation is 51.8 mm. The ground surface settlement curves of excavation section ($x = 0$ m), the section 15 m behind excavation face

Table 3: Physical and mechanical parameters of existing shield tunnel.

Material	Elastic modulus E (MPa)	Intersegment shear stiffness k_t (kN·m^{-1})	Poisson's ratio μ	Bulk density γ (kN·m^{-3})	Outer diameter (m)	Thickness (m)	Segment width (m)
Existing shield tunnel	37600	400000	0.25	24	6.2	0.35	1
New tunnel segments	37600	—	0.25	24	—	0.35	1.5
Shield cutter	205000	—	0.22	29	—	0.5	—
Shield shell	140000	—	0.22	29	—	7	—

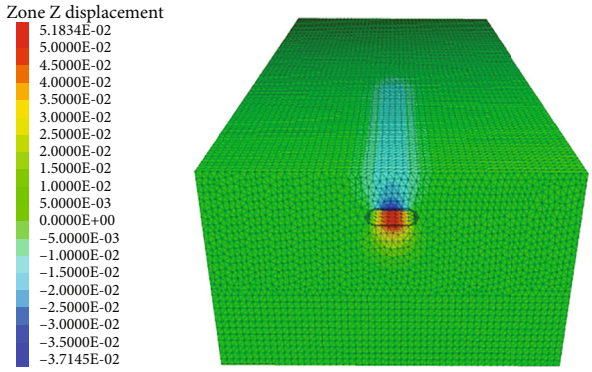

Figure 12: Ground surface subsidence cloud map.

($x = -15$ m), and the section 15 m in front of excavation face ($x = 15$ m) are shown in Figure 13.

The following can be obtained from Figure 13:

(1) Ground surface subsidence is distributed symmetrically about new tunnel's central axis, in which the maximum subsidence position of cross-section occurs. Error values of results by numerical simulation, theoretical calculation, and field monitoring are small, which verifies their correctness. The maximum ground surface settlement is about 15 mm, which meets construction control standard (the maximum settlement is less than 30 mm)

(2) At a section of 15 m in front of excavation face ($x = 15$ m), the surface is slightly uplifted and deformed, which is induced by frontal thrust of shield machine. The ground surface behind excavation face has subsidence deformation, and the maximum settlement position is about 4 times the length of shield shell from cutter. Stratum loss is the main cause of ground subsidence, followed by shield friction resistance, while additional frontal thrust and additional grouting pressure have little effect on ground subsidence

6.4.2. Ground Surface Deformation Analysis. Figure 14 shows deformation of existing shield tunnel below when quasirectangular shield tunneling. The following can be obtained:

(1) Error between numerical simulation calculation results and theoretical calculation results is small, which verifies that it is feasible to use the shear stagger model to simulate existing shield tunnel. However, theoretical calculation results show that disturbance range of new quasirectangular tunnel on existing shield tunnel is wider, because the stratum is considered as a semi-infinite elastic space body in the theoretical calculation, and the transfer consumption of the additional load caused by the plastic properties of the stratum is ignored, so that the calculated disturbance range is wider. Theoretical calculation method is effective to predict deformation of new tunnel within twice the diameter of existing shield tunnel near central axis

(2) When new tunnel face is located behind existing shield tunnel, the existing shield tunnel will deform downward by the additional frontal thrust. When new tunnel passes through existing shield tunnel, deformation of existing shield tunnel changes from downward deformation to uplift deformation. Since the spatial orthogonal relationship between those two tunnels is applied, deformation of existing shield tunnel is distributed symmetrically

To simply analyze deformation of existing shield tunnel under external disturbances, many scholars regard existing shield tunnel as elastic foundation beams to reduce the amount of calculation [23–26]. According to the method in the article, this paper compares the calculation method of elastic foundation beam and calculation method of shear stagger model. This paper compares lateral deformation of existing shield tunnel caused by new tunnel excavation directly above existing shield tunnel and its maximum deformation during quasirectangular shield tunneling, as shown in Figure 15.

(1) From Figure 15(a), the deformation trend of existing shield tunnel is consistent: When new tunnel is excavated right above existing shield tunnel, the existing shield tunnel is uplifted deformed, and the deformation curve is in the shape of an inverted "V." The maximum bulge of the arched curve is at $x = 0$ m, right above the axis of new tunnel. Results calculated by shear stagger model hold the best fit with results of numerical simulation. Deformation calculation

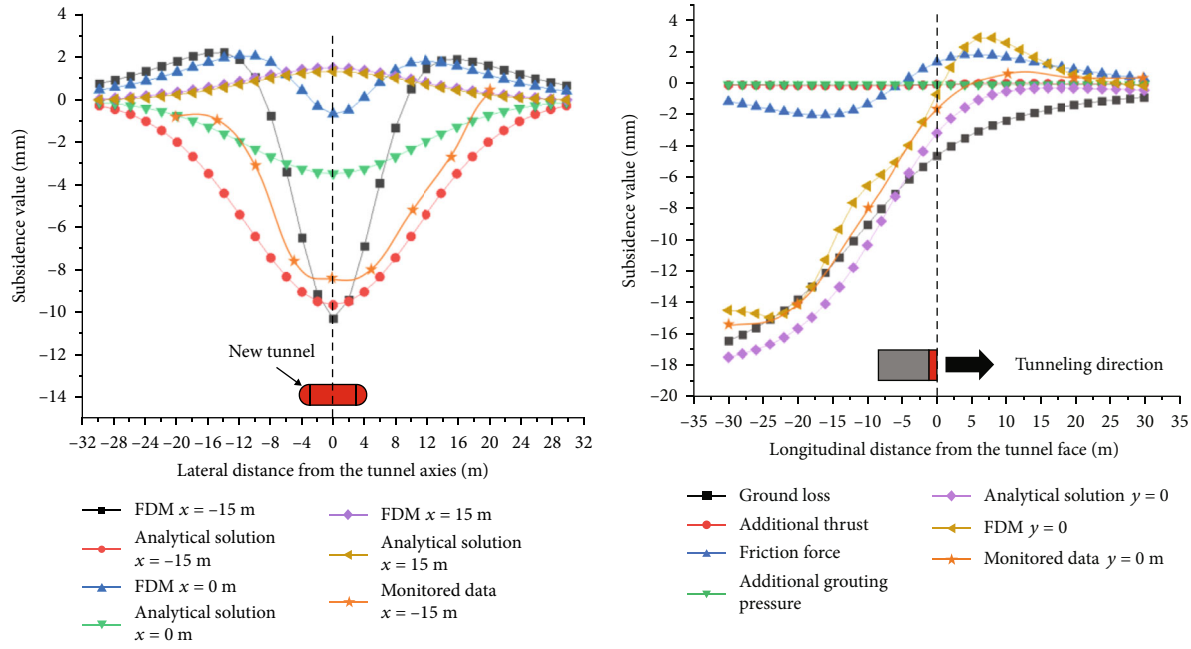

(a) Lateral subsidence curve

(b) Longitudinal subsidence curve

Figure 13: Subsidence curve.

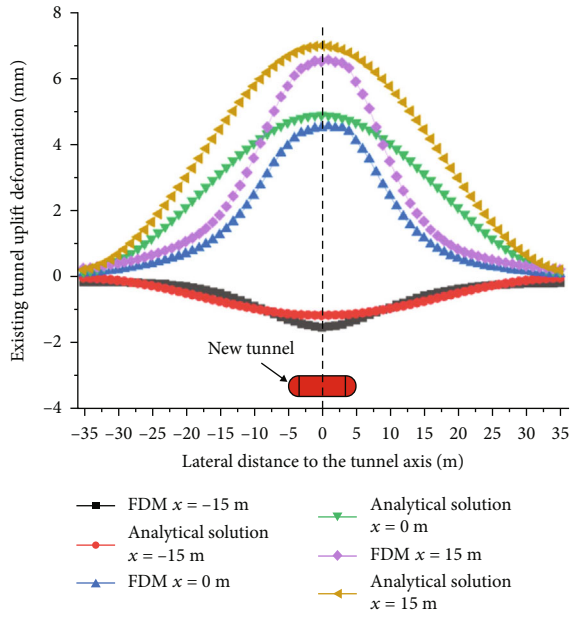

Figure 14: Lateral deformation curve of existing shield tunnel.

results of the existing shield tunnel have small errors, and the width of the uplift arch is similar. It is proved that it is reliable to use the shear stagger model to calculate deformation of existing shield tunnel due to construction disturbance. In contrast, the calculation results and numerical simulation results by continuous elastic beams have poor fit, because the shear discontinuity of the existing shield tunnel is not considered when using continuous elastic beams method, so that the results are too large, and the width of the uplift arch increases

(2) From Figure 15(b), deformation at the longitudinal center point of existing shield tunnel is consistent with shield tunneling: With excavation of the quasirectangular tunnel, deformation at longitudinal center of existing shield tunnel increases smoothly. When excavation distance reaches 35 m ($x = 15$ m), the deformation of existing shield tunnel begins to increase sharply. When tunnel excavation distance is 70 m ($x = -22.5$ m), the stable deformation occurs. Since tunnel face is far away from the existing shield tunnel when new tunnel starts to be excavated, the deformation of existing shield tunnel under construction disturbance is small, and the three calculation results are similar. However, as the tunnel face approaches the existing shield tunnel, results obtained by the Winkler foundation beam calculation become larger and are quite different from the other two calculation results. The calculation results of the shear stagger model are similar to the numerical simulation results. Results of Winkler foundation beam model show that disturbance effect on existing shield tunnel increases when new tunnel is excavated to the range of $x = -22.5 \sim 22.5$ m

6.4.3. Analysis of Segment Stagger Amount of Existing Shield Tunnel. The segment stagger amount of shield tunnels and the rotation angle between segments are related to safety of tunnel and waterproof system. The greater the amount of stagger and splay between segments is, the greater the probability of water leakage in tunnel increases. Therefore,

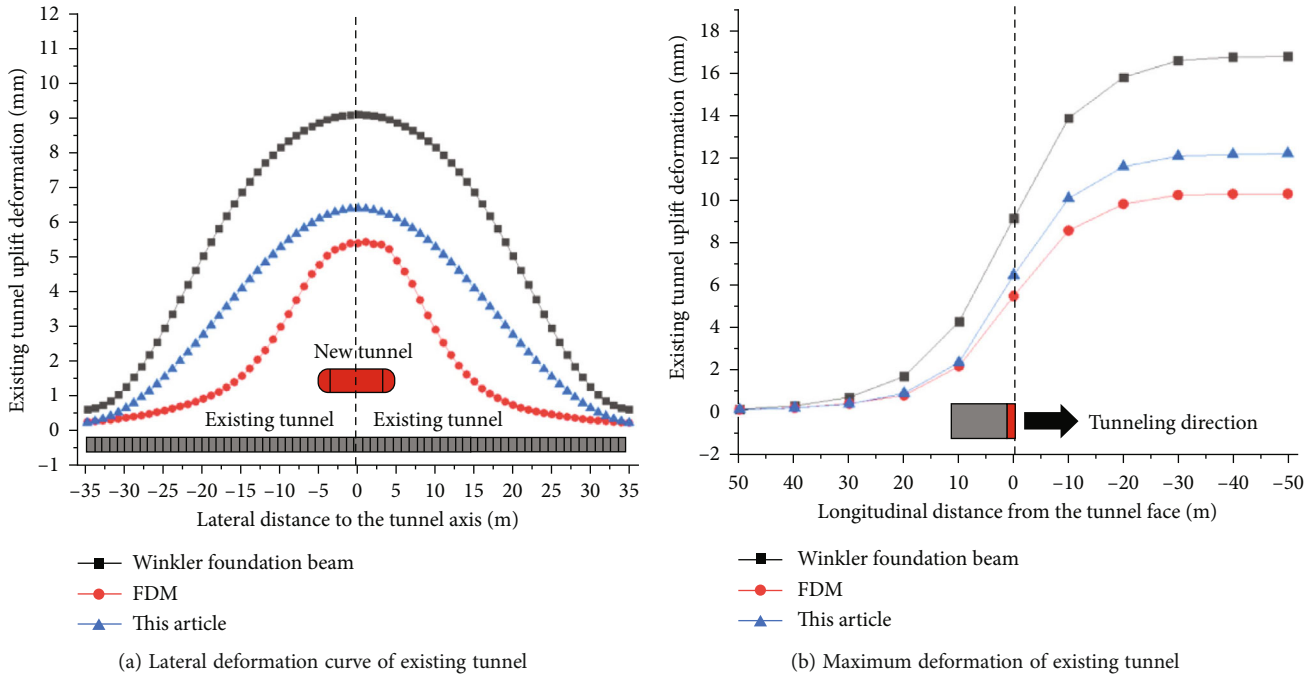

(a) Lateral deformation curve of existing tunnel

(b) Maximum deformation of existing tunnel

Figure 15: Comparison of existing shield tunnel deformation calculation.

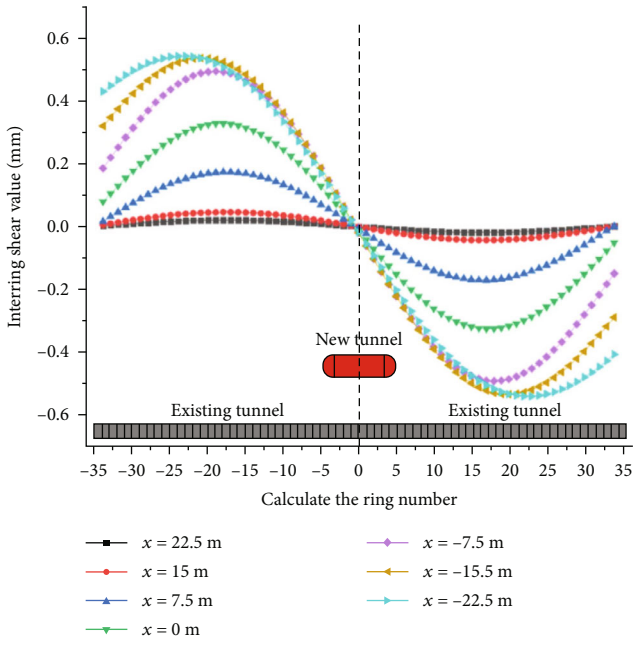

Figure 16: Variation curve of the amount of dislocation platform of existing shield tunnel pieces.

estimating misalignment of tunnels is necessary. Using the shear stagger model, the stagger amount of the existing shield tunnel segments, rotation angle between segments, and shear force can be calculated at the same time. Figure 16 is a variation curve of segment stagger of existing shield tunnel with distance from the axis of new tunnel. As new tunnel is excavated, the amount of segment stagger increases gradually. When the tunnel excavation distance is 70 m ($x = -22.5$ m), the segment stagger reaches constant value. The maximum stagger occurs at inflection point of the uplift deformation curve of existing shield tunnel, and the maximum value is 0.55 mm. The minimum stagger is at position with the maximum uplift deformation of existing shield tunnel, and the value is 0 mm, where basically no segment stagger. The amount of segment stagger has an important impact on structural stability and impermeability of existing shield tunnel. Excessive segment stagger may cause segment cracking, joint leakage, etc. Calculating the segment stagger can provide guidance for monitoring and measurement in similar projects.

6.4.4. Analysis of Shear Force between Segments of Existing Tunnel. New tunnel construction will cause stagger deformation between segments of existing shield tunnel, and the bolts between segments will bear a large shear force between the segments in order to resist the deformation. Structural failure occurs when the shear force exceeds shear strength limit of the bolt, so it is particularly important to calculate the shear force between segments. Figure 17 shows variation curve of the shear force between segments calculated by shear stagger model. From Figure 17, the shear force between existing shield tunnel segments is symmetrically distributed at the longitudinal center point of existing shield tunnel. When segments of existing shield tunnel approach the axis of new tunnel, the shear force first increases and then decreases. Shear force reaches maximum value at inflection point of existing shield tunnel deformation curve and reaches the minimum value at position with existing shield tunnel's maximum uplift deformation. As excavation distance of new tunnel increases, the shear force between the segments of the existing shield tunnel increases

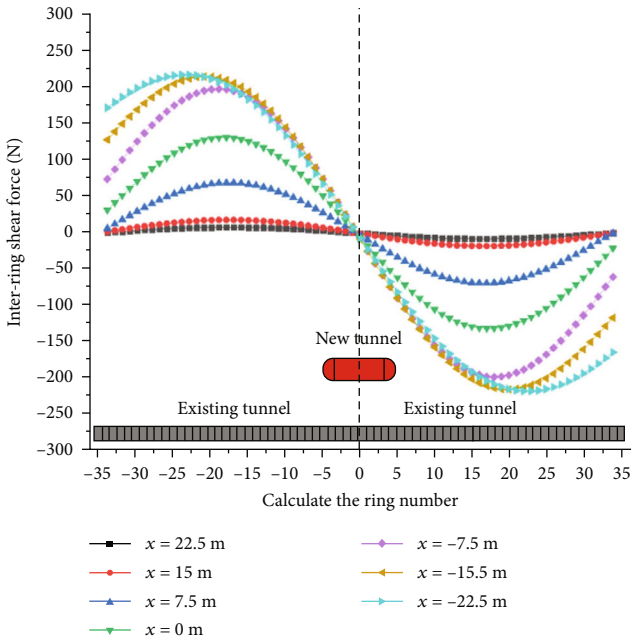

Figure 17: Shearing force between shield tunnel segments.

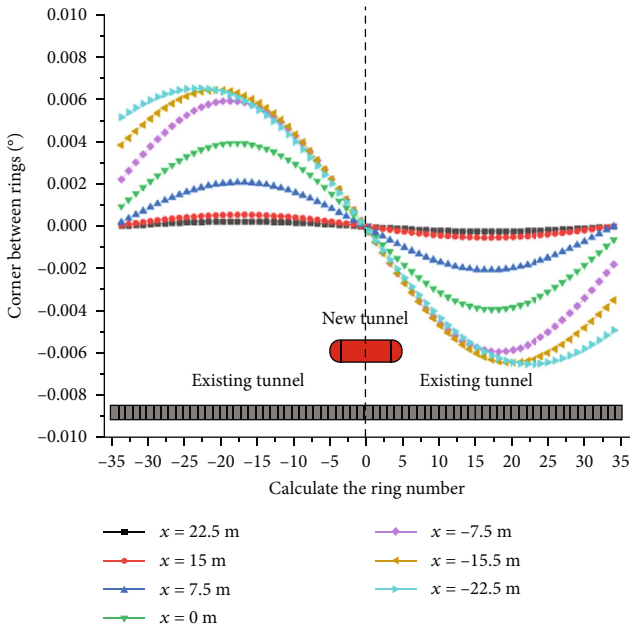

Figure 18: Rotation angle between shield tunnel rings.

gradually. When excavation distance reaches 70 m ($x = -22.5$ m), the shear force between segments reaches constant value. According to design of the existing shield tunnel, 17 carbon steel anchor bolts with a diameter of 20 mm are used to connect segments, and the allowable shear strength is 178 MPa. It can be obtained from the figure that the maximum shear force is about 230 N, and the maximum shear stress of the bolt is calculated to be 61 MPa, which is far lower than the allowable bearing shear strength. Therefore, tunnel construction will not cause the bolt failure of existing shield tunnel.

6.4.5. Analysis of Rotation Angle between Segments of Existing Shield Tunnel. As shown in Figure 18, the segment near the maximum longitudinal settlement of tunnel does not have rotational transformation as rigid body. However, at the inflection point of tunnel's horizontal displacement, the segment rotation angle reaches the maximum, and the maximum rotation angle is 0.0071°. The variation trend of segment stagger and segment rotation angle and shear force between segments is the same.

7. Conclusion

In this paper, the mirror image method and the Mindlin solution are used to calculate additional stress at axis of existing shield tunnel under the influence of stratum loss, shield front thrust, shield friction, and grouting pressure. Based on shear stagger model, the minimum potential energy principle is used to obtain the variation curves of existing shield tunnel deformation, the segment stagger amount, the shear force between segments, and the segment splay amount with the new tunnel excavation. The analytical prediction results are verified by an FEM and on-site monitoring data. The results show the following:

(1) Errors among the on-site monitoring data, the FEM calculation results, and the analytical calculation results are small, which verifies practicality of FEM and analytical calculation formula. Maximum subsidence of ground surface, maximum deformation of existing shield tunnel, maximum shear stagger, maximum splay, and maximum shear force, respectively, all meet construction control requirements

(2) Lateral settlement of the ground is symmetrically distributed, causing slight uplift deformation in front of excavation face and subsidence behind excavation face. Distance from excavation face to the maximum settlement position is about 4 times the length of shield shell. Stratum loss is the main cause of ground subsidence, followed by shield friction resistance, while the frontal thrust and grouting pressure have little effect on ground subsidence

(3) Error between the maximum deformation of existing shield tunnel calculated by the Winkler foundation beam method and the numerical calculation result is 68%, while the error of the calculation result using the shear stagger model is 18%, indicating that the shear stagger model is more accurate and reliable. Moreover, the shear stagger model can also analyze the variation of the segment stagger amount, the shear force between the segments, and the segment splay

(4) Existing shield tunnel deformation, segment stagger, shear force between the segments, and segment splay gradually increase with new tunnel excavation and tend to be stable after shield machine passes through existing shield tunnel for 22.5 m. The amount of segment stagger, shear force

between the segments, and segment splay reaches the maximum value at the inflection point of deformation curve and reaches the minimum value at position with the maximum uplift deformation of existing shield tunnel, whose change trends are the same

(5) In the process of theoretical calculation, the stratum is regarded as homogeneous stratum, but the actual stratum is layered. Horizontal displacement of existing shield tunnel is not analyzed in this paper. Inhomogeneous distribution of the front thrust of shield, friction force of shield shell, and grouting force of shield tail is not considered during tunnel construction, which need further researches in the future

Data Availability

The data used to support the findings of this study are available from the corresponding author upon request.

Conflicts of Interest

No potential conflict of interest was reported by the authors.

Acknowledgments

This study was supported by the Natural Science Foundation of the Higher Education Institutions of Jiangsu Province of China grant number 20KJB560006.

References

[1] W. Zhang, W. De Corte, X. Liu, and L. Taerwe, "Influence of rotational stiffness modeling on the joint behavior of quasi-rectangular shield tunnel linings," *Applied Sciences*, vol. 10, no. 23, p. 8396, 2020.

[2] V. V. Pham, N. A. Do, and D. Dias, "Sub-rectangular tunnel behavior under seismic loading," *Applied Sciences*, vol. 11, no. 21, p. 9909, 2021.

[3] S. Li, Y. Zhang, M. Cao, and Z. Wang, "Study on excavation sequence of pilot tunnels for a rectangular tunnel using numerical simulation and field monitoring method," *Rock Mechanics and Rock Engineering*, vol. 55, no. 6, pp. 3507–3523, 2022.

[4] V. Avgerinos, D. M. Potts, and J. R. Standing, "Numerical investigation of the effects of tunnelling on existing tunnels," *Géotechnique*, vol. 67, no. 9, pp. 808–822, 2017.

[5] B. Liu, Z. Yu, R. Zhang, Y. Han, S. Wang, and S. Wang, "Effects of undercrossing tunneling on existing shield tunnels," *International Journal of Geomechanics*, vol. 21, no. 8, article 04021131, 2021.

[6] R. Liang, C. Kang, L. Xiang, Z. Li, and Y. Guo, "Responses of in-service shield tunnel to overcrossing tunnelling in soft ground," *Environmental Earth Sciences*, vol. 80, no. 5, pp. 1–15, 2021.

[7] L. Wu, X. Zhang, Z. Zhang, and W. Sun, "3D discrete element method modelling of tunnel construction impact on an adjacent tunnel," *KSCE Journal of Civil Engineering*, vol. 24, no. 2, pp. 657–669, 2020.

[8] H.-N. Wu, S.-L. Shen, S.-M. Liao, and Z.-Y. Yin, "Longitudinal structural modelling of shield tunnels considering shearing dislocation between segmental rings," *Tunnelling and Underground Space Technology*, vol. 50, pp. 317–323, 2015.

[9] H. Lai, H. Zheng, R. Chen, Z. Kang, and Y. Liu, "Settlement behaviors of existing tunnel caused by obliquely undercrossing shield tunneling in close proximity with small intersection angle," *Tunnelling and Underground Space Technology*, vol. 97, p. 103258, 2020.

[10] H.-S. Deng, H.-L. Fu, S. Yue, Z. Huang, and Y.-Y. Zhao, "Ground loss model for analyzing shield tunneling-induced surface settlement along curve sections," *Tunnelling and Underground Space Technology*, vol. 119, p. 104250, 2022.

[11] T. E. Vorster, A. Klar, K. Soga, and R. J. Mair, "Estimating the effects of tunneling on existing pipelines," *Journal of Geotechnical & Geoenvironmental Engineering*, vol. 131, no. 11, pp. 1399–1410, 2005.

[12] D.-M. Zhang, Z.-K. Huang, Z.-L. Li, X. Zong, and D.-M. Zhang, "Analytical solution for the response of an existing tunnel to a new tunnel excavation underneath," *Computers and Geotechnics*, vol. 108, pp. 197–211, 2019.

[13] Z. Zhou, Y. Chen, Z. Liu, and L. Miao, "Theoretical prediction model for deformations caused by construction of new tunnels undercrossing existing tunnels based on the equivalent layered method," *Computers and Geotechnics*, vol. 123, article 103565, 2020.

[14] C. Sagaseta, "Analysis of undrained soil deformation due to ground loss," *Geotechnique*, vol. 37, no. 3, pp. 301–320, 1987.

[15] R. D. Mindlin, "Force at a point in the interior of a semi-infinite solid," *Physics*, vol. 7, no. 5, pp. 195–202, 1936.

[16] H. Tanahashi, "Formulas for an infinitely long Bernoulli-Euler beam on the Pasternak model," *Soils and foundations*, vol. 44, pp. 109–118, 2004.

[17] S. Shivaei, N. Hataf, and K. Pirastehfar, "3D numerical investigation of the coupled interaction behavior between mechanized twin tunnels and groundwater - a case study: Shiraz metro line 2," *Tunnelling and Underground Space Technology*, vol. 103, p. 103458, 2020.

[18] P.-T. Simic-Silva, B. Martínez-Bacas, R. Galindo-Aires, and D. Simic, "3D simulation for tunnelling effects on existing piles," *Computers and Geotechnics*, vol. 124, p. 103625, 2020.

[19] Z. Zhang and M. Huang, "Geotechnical influence on existing subway tunnels induced by multiline tunneling in Shanghai soft soil," *Computers and Geotechnics*, vol. 56, pp. 121–132, 2014.

[20] R. Zhou, W. Fang, and J. Wu, "A risk assessment model of a sewer pipeline in an underground utility tunnel based on a Bayesian network," *Tunnelling and Underground Space Technology*, vol. 103, p. 103473, 2020.

[21] R. Liang, T. Xia, M. Huang, and C. Lin, "Simplified analytical method for evaluating the effects of adjacent excavation on shield tunnel considering the shearing effect," *Computers and Geotechnics*, vol. 81, pp. 167–187, 2017.

[22] D. Lu, F. Kong, X. Du, C. Shen, Q. Gong, and P. Li, "A unified displacement function to analytically predict ground deformation of shallow tunnel," *Tunnelling and Underground Space Technology*, vol. 88, pp. 129–143, 2019.

[23] H. Deng, H. Fu, Y. Shi, Z. Huang, and Q. Huang, "Analysis of asymmetrical deformation of surface and oblique pipeline caused by shield tunneling along curved section," *Symmetry*, vol. 13, no. 12, p. 2396, 2021.

[24] Z. Zhang, Y. Pan, M. Zhang, X. Lv, K. Jiang, and S. Li, "Complex variable analytical prediction for ground deformation and lining responses due to shield tunneling considering groundwater level variation in clays," *Computers and Geotechnics*, vol. 120, article 103443, 2020.

[25] M. Zhang, S. Li, and P. Li, "Numerical analysis of ground displacement and segmental stress and influence of yaw excavation loadings for a curved shield tunnel," *Computers and Geotechnics*, vol. 118, article 103325, 2020.

[26] S. Ye, Z. Zhao, and D. Wang, "Deformation analysis and safety assessment of existing metro tunnels affected by excavation of a foundation pit," *Underground Space*, vol. 6, no. 4, pp. 421–431, 2021.